Structure of p73 DNA-binding domain tetramer modulates p73 transactivation

Abdul S. Ethayathulla[a], Pui-Wah Tse[a], Paola Monti[b], Sonha Nguyen[a], Alberto Inga[c], Gilberto Fronza[b], and Hector Viadiu[a,1]

[a]Laboratory of Structural Biochemistry, Department of Chemistry and Biochemistry, University of California at San Diego, 9500 Gilman Drive 0378, La Jolla, CA 92093; [b]Molecular Mutagenesis and DNA Repair Unit, Department of Epidemiology and Prevention, Instituto di Ricerca e Cura A Carattere Scientifico, Azienda Ospedaliera Universitaria San Martino—Instituto Scientifico Tumori Instituto Nazionale per la Ricerca sul Cancro, Largo Rosanna Benzi, 10, 16132 Genoa, Italy; and [c]Laboratory of Transcriptional Networks, Centre for Integrative Biology, 38060 Trento, Italy

Edited by Carol Prives, Columbia University, New York, NY, and approved February 17, 2012 (received for review September 21, 2011)

The transcription factor p73 triggers developmental pathways and overlaps stress-induced p53 transcriptional pathways. How p53-family response elements determine and regulate transcriptional specificity remains an unsolved problem. In this work, we have determined the first crystal structures of p73 DNA-binding domain tetramer bound to response elements with spacers of different length. The structure and function of the adaptable tetramer are determined by the distance between two half-sites. The structures with zero and one base-pair spacers show compact p73 DNA-binding domain tetramers with large tetramerization interfaces; a two base-pair spacer results in DNA unwinding and a smaller tetramerization interface, whereas a four base-pair spacer hinders tetramerization. Functionally, p73 is more sensitive to spacer length than p53, with one base-pair spacer reducing 90% of transactivation activity and longer spacers reducing transactivation to basal levels. Our results establish the quaternary structure of the p73 DNA-binding domain required as a scaffold to promote transactivation.

The p73 transcription factor that belongs to the p53 protein family and participates in pheromonal sensory, chromosome stability, neurogenesis, inflammation, and osteoblastic differentiation pathways (1, 2). In contrast to p53, p73 is mutated in less than 0.5% of human tumors (3); however, it also participates in p53-dependent and independent pathways, showing oncogenic and tumor suppressor functions (4, 5). These dual opposite activities are due to the presence of two promoters which results in the expression of two main isoforms, TAp73 and ΔNp73 (6).

How the members of the p53 protein family trigger different cellular responses still remains an open question. Overall, p73 and p63 can bind to the same p53 response elements (REs), but the activated pathways are different (7, 8). There is some redundancy in the activation of stress pathways by the three members of the p53 protein family, but, at the same time, over 100 genes regulated by p73 and p63 are not activated by p53 (9, 10). Like p53, p73 also binds to a 20-bp RE, comprising two half-site decamers in direct orientation that follow a 5′-Pur1-Pur2-Pur3-Cyt4-Ade5/Thy5-Ade6/Thy6-Gua7-Pyr8-Pyr9-Pyr10-3′ consensus sequence (10, 11). Half of the known p53 REs do not have any insertion between the two half-sites and spacers larger than 3 bp are rare, particularly among sites that are transcriptionally activated (12–14). In the case of p53 repressed genes, the *cis*-element code is poorly defined, but based on a limited number of examples, spacer length appears to be more uniformly distributed and targets have no preference for 0-bp spacers (12).

Human p73α is a 636 amino acid protein with a tripartite domain organization similar to its close homolog, p63, and to the shorter 393 amino acid long p53 protein. Members of the p53 family have a disordered N-terminal transactivation domain, a central immunoglobulin-like DNA-binding domain (DBD), and a C terminus that starts with a domain that promotes oligomerization. In p53, the last 30 amino acids form a regulatory domain that binds DNA nonspecifically, whereas p73 and p63 have more than 200 extra amino acids that include a protein–protein interaction sterile alpha-motif domain. The DBD is the most conserved domain with 58% sequence identity between p73 and p53 (Fig. 1*A*). The first structure of p53 DBD bound to DNA showed a loop-sheet-helix motif contacting the bases and the phosphate backbone of one quarter-site RE (15). More recent structures of p53 and p63 DBDs in complex with DNA have shown a dimer of DBD dimers where each monomer binds to one of the four basic 5-bp inverted repeat recognition sequences, creating dimerization and tetramerization interfaces (16–23), but no structure of p73 in complex with DNA is known.

In spite of the structural knowledge accumulated, the molecular mechanism of differential transcriptional activation by p53-protein-family members remains largely unexplained. Spacer length between RE half-sites plays an important activator role to trigger apoptotic or nonapoptotic pathways (12, 24). We determined the crystal structures of p73 DBD tetramer in complex with different REs. For REs with different spacer lengths, we studied the structural basis of p73 DBD oligomerization and DNA binding and, using a yeast-based functional assay, we measured the spacer length effect on the transactivation levels induced by p73 and p53. Our results describe the oligomerization state and the changes in p73 DBD quaternary structure and DNA conformation as a function of RE spacer length, measure DNA-binding, and establish that transcriptional activity is affected more by spacer length in p73 than in p53.

Results

Crystal Structures of p73 DNA-Binding Domain with 0,1, 2, and 4 Base-Pair Spacers. Cocrystallization experiments between p73 DBD and oligonucleotides carrying half-site REs were performed with a 198 amino acid protein construct from residues 115 to 312 of human full-length p73. We determined the crystal structure of p73 DBD in complex with DNA in three crystal forms. The structures were solved by molecular replacement using a p53 DBD dimer–DNA complex as a search model and final refined structures were determined (*SI Text* and Table S1). The crystal structures of p73 DBD, as in the case of p53 and p63 DBDs structures, show an immunoglobulin-like β-sandwich fold with two antiparallel β-sheets (Fig. 1*B* and Fig. S1). One β-sheet has four β-strands (S1, S3, S5, and S8) and the other has five β-strands (S4, S6, S7, S9, and S10). Three long loops emerge from the core β-sandwich fold. Loop L1 links β-strands S1 and S3 and contains two

Author contributions: A.S.E., A.I., G.F., and H.V. designed research; A.S.E., P.-W.T., P.M., S.N., G.F., and H.V. performed research; A.S.E., P.-W.T., P.M., A.I., G.F., and H.V. analyzed data; and A.S.E., A.I., G.F., and H.V. wrote the paper.

The authors declare no conflict of interest.

This article is a PNAS Direct Submission.

Data deposition: The atomic coordinates and structure factors have been deposited in the Protein Data Bank, www.pdb.org (PDB ID codes 3VD0, 3VD1, and 3VD2).

[1]To whom correspondence should be addressed. E-mail: viadiu@ucsd.edu.

This article contains supporting information online at www.pnas.org/lookup/suppl/doi:10.1073/pnas.1115463109/-/DCSupplemental.

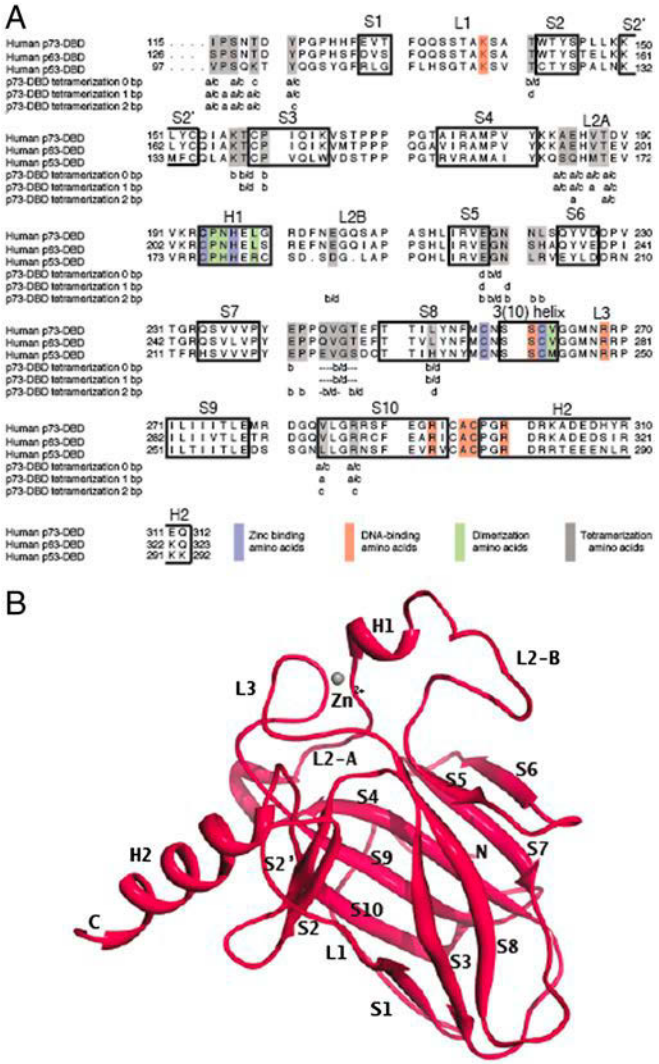

Fig. 1. Primary, secondary, and tertiary structure of human p73 DBD. (*A*) Sequence alignment of human DBDs of p53 protein family. Residues forming each secondary structure element are enclosed in boxes. Residues involved in zinc binding (blue), DNA binding (orange), dimerization (green), and tetramerization (gray) are highlighted. For the residues in the tetramerization interface of structures with 0-, 1-, and 2-bp RE spacers, the monomers contributing to the tetramerization interface are listed. (*B*) Protein-fold of p73 DBD. Secondary structure elements, polypeptide termini, and the zinc atom are labeled.

small β-strands, S2 and S2′, that pack against S10 and H2. The long loop L2, divided in L2A and L2B, has α-helix H1 and has a two amino acid insertion with respect to p53. Loop L3 extends from S8 to S9. A Zn^{2+} ion, crucial for dimerization and DNA binding, is tetrahedrally coordinated by Cys194 and His197 from α-helix H1 and Cys258 and Cys262 from loop L3. DNA is bound by a loop-sheet-helix motif formed by L1, L3, S10, and H2. The structure of the p73 DBD to 1.8-Å resolution in the absence of DNA has been deposited in the Protein Data Bank (2XWC; Alex Bullock Laboratory at Structural Genomics Consortium, Oxford University). The rmsd between the positions of the C^{α} of p73 DBD with and without DNA is 0.8 Å. The small differences are in the loops involved in tetramerization and DNA binding, particularly residues Gly265, Met266, and Asn267 are disordered in the absence of DNA and become ordered upon binding to DNA. Overall, the DBD of the members of the p53 protein family are structurally related.

Considering crystal packing, the three solved crystal forms contain five unique quaternary arrangements. The three oligonucleotides used in crystallization have closely related half-site consensus sequences, each with two identical inverted RE quarter-sites, plus one or two flanking nucleotides (Fig. 2). In the asymmetric unit of crystal 1 and 2 with 12 bp oligonucleotides, two unique tetramers bind to a central 20-bp RE (Fig. S2 *A* and *B*). The first tetramer is different in each crystal form: in crystal 1, tetramer formation displaces two base pairs, one at the end of each stacked oligonucleotide, resulting in a tetramer bound to a 0-bp spacer RE (Fig. 2*A*); in crystal 2, the tetramer displaces only one base pair at the juncture of both stacked oligonucleotides, resulting in a tetramer bound to a 1-bp spacer RE (Fig. 2*B*). The second tetramer in the asymmetric unit has an identical arrangement in both crystals without displacing any base pairs; both oligonucleotides stack on top of each other to form a tetramer complexed to a 2-bp spacer RE (Fig. 2*C*). In crystal 3, the asymmetric unit contains three identical p73 DBD dimers bound to three 14 bp oligonucleotides where dimers separated by 4 bp do not form a dimer–dimer interface (Fig. 2*D* and Fig. S2*C*). The DNA packing in the three crystals forms (Fig. S2 *D* and *E*) results in the stacking of two oligonucleotides to form a double-stranded full-length RE with continuous electron density (Fig. S3); the existence of a continuous DNA density was confirmed by analyzing the DNA conformation and carrying out extra refinement steps with the DNA ends joined to model entire REs for each tetramer in the three crystal forms (Fig. S4).

The p73 DBD Recognizes Different REs in a Structurally Similar Manner. To understand how p73 DBD binds DNA, we studied its oligomerization by analytical ultracentrifugation. Sedimentation velocity experiments demonstrated that p73 DBD is a monomer in the absence of DNA and it dimerizes upon DNA binding (Fig. 3*A*). In the absence of DNA, the isolated p73 DBD is a monomer with a 2.1 S sedimentation coefficient. However, experiments with fluorescein-labeled oligonucleotides of different lengths containing either half- (12 or 14 bp) or full-site REs

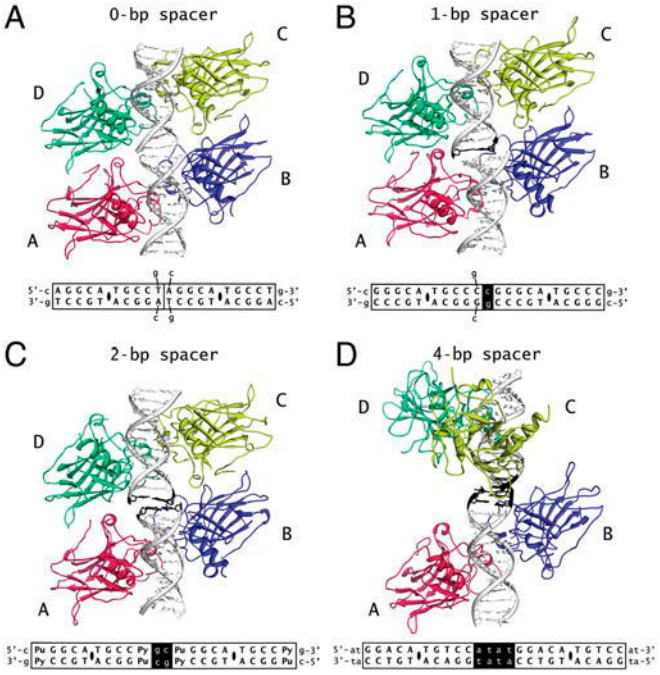

Fig. 2. Crystal structures of p73 DBD in complex with DNA. (*A*) Tetramer bound to two 12 bp oligonucleotides forming an RE with 0-bp spacer with two base pairs flipped out of the DNA double helix. (*B*) Tetramer bound to two 12 bp oligonucleotides forming an RE with 1-bp spacer (in black) with one base pair flipped out of the DNA double helix. (*C*) Tetramer bound to two 12 bp oligonucleotides forming an RE with 2-bp spacer (in black). (*D*) Dimers bound to a 14 bp oligonucleotide with half-site RE. Two oligonucleotides stack to form a RE with a 4-bp spacer (in black) with dimers not forming a tetramer.

(20 or 24 bp) show that p73 DBD first binds to DNA as a dimer with a sedimentation coefficient between 3.4 and 4.2 S and, when the oligonucleotide includes a full RE, besides the dimer, a DNA-bound tetramer with a sedimentation coefficient between 6.5 and 6.8 S appears. The oligomeric forms observed in the crystal packing of p73 DBD in complex with DNA are consistent with the hydrodynamic experiments (Figs. 2 and 3*A*).

To understand p73 DBD DNA-binding properties and the effect of space length in DNA binding, we studied the three half-site RE sequences used in the crystallization and four full-site RE sequences with 0-, 1-, 2-, and 4-bp spacers by fluorescence anisotropy (Fig. 3*B* and Fig. S5). A p73 DBD dimer recognizes a half-site that follows the 5′-Pur1-Pur2-Pur3-Cyt4-Ade5/Thy5-Ade6/Thy6-Gua7-Pyr8-Pyr9-Pyr10-3′ consensus rule. The p73 DBD dissociation constants obtained for p73 DBD dimer binding to the half-site RE sequences used for crystallization were similar, demonstrating that purine/purine substitutions in the first and third base pairs result in equivalent binding (Fig. 3*B* and Fig. S5). Importantly, the p73 oligomerization domain has an essential contribution to DNA affinity, as already observed for p53 (21, 25). These values are also comparable to the ones observed for p63 DBD (22).

The interactions between p73 DBD and DNA involve residues from a loop-sheet-helix motif (L1-S10-H2) to the DNA bases and backbone, plus interactions of loop L3 with the DNA backbone (Fig. 3*C*). Approaching from the DNA major groove, Arg300, Cys297, and Lys138 reach the DNA major groove to contact the DNA bases Gua4′, Cyt3′, and Gua2/Ade2, respectively (Fig. 3*D*). The cytosine in position four is the most conserved base of the quarter recognition site because its complementary base Gua4′ has two atoms, O6 and N7, sharing hydrogen bonds with the Arg300 guanidinium group. Purine degeneracy at positions two and three of the consensus site is due to the flexibility of Cys297 and Lys138. The sulfhydryl group from Cys297 is a hydrogen-bond acceptor to the N4 of Cyt3′ in crystal 1 and 2 and a hydrogen-bond donor to the O4 of Thy3′ in some monomers in crystal 3; although Lys138 is always hydrogen bonding to N7 of Gua2 in all the crystals forms, it is found in some monomers keeping multiple hydrogen bonds that also include the O6 of Gua3. No direct contacts are observed to the bases in positions one and five. Besides the described contacts to the DNA bases, five contacts to the DNA phosphates stabilize the complex: the amide groups of Lys138 and Ala296 and the minor-groove-approaching side chains of Ser261, Arg268, and Arg293 in strand S10. The average distance found between the C1′ atoms of the central A-T base pairs in all the crystal forms is about 10 Å, which is closer to the ideal Watson–Crick distance (Fig. S3*E*). The central A-T base pair was modeled as a Watson–Crick base pair because the 2.9-Å resolution of our maps did not allow us to observe the likely flip of the central Ade5 to a Hoogsteen base-pair conformation as it has been described for p53 (20).

Dependence of p73 Transactivation Activity on RE Spacer Length. RE spacer length is an important regulatory mechanism in the p53 protein family (12). ChIP and microarray experiments have shown that p73 activates at least 85 genes, 27 of which are also activated by p53 (26). For the 85 genes activated by p73, the p53FamTaG database lists 266 p73 REs with a wide range of conservation of the consensus motif (27). Of the 50 p73 REs that have a conserved central CATG motif in both half-sites, 82%

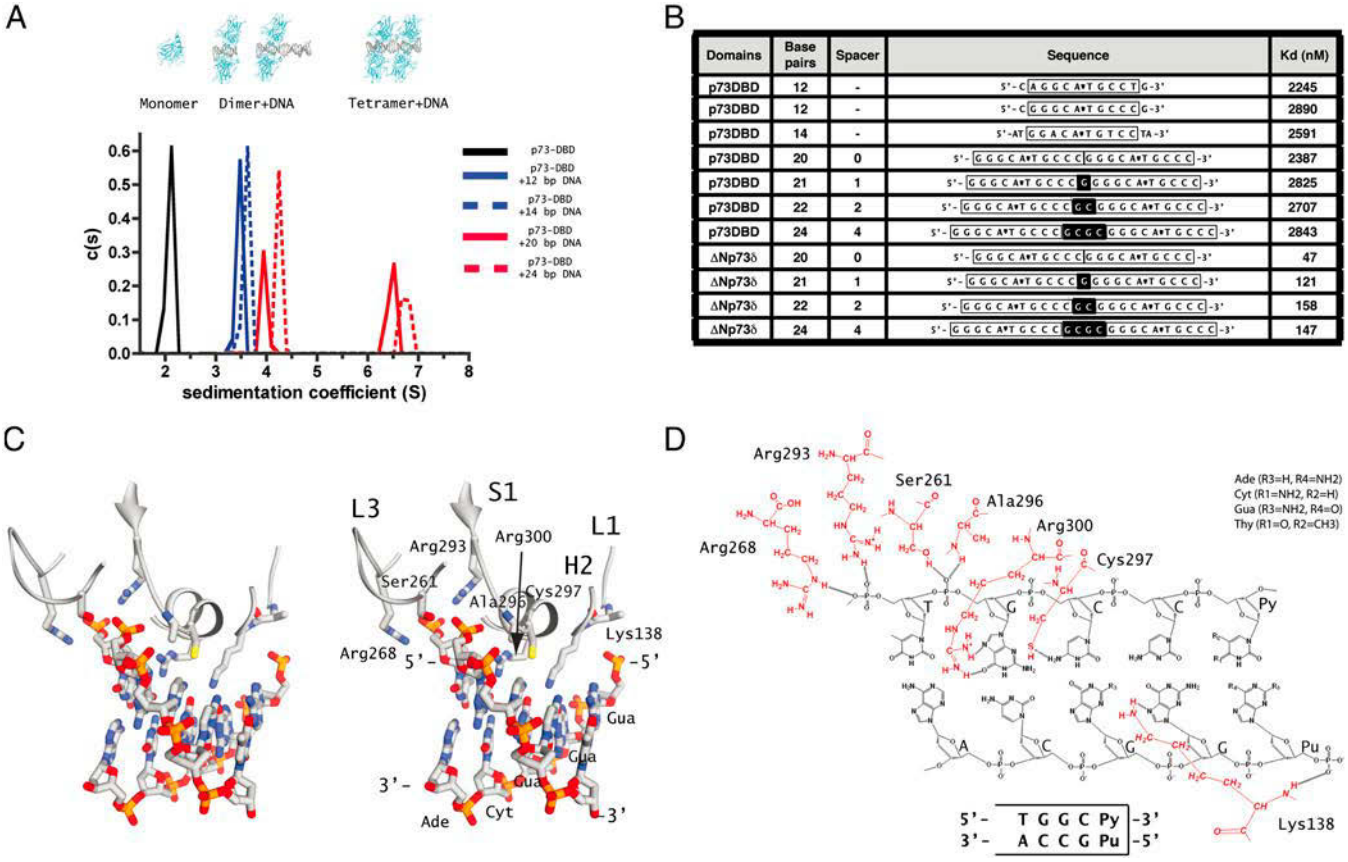

Domains	Base pairs	Spacer	Sequence	Kd (nM)
p73DBD	12	-	5′-C A G G C A•T G C C T G-3′	2245
p73DBD	12	-	5′-C G G G C A•T G C C C G-3′	2890
p73DBD	14	-	5′-AT G G A C A•T G T C C TA-3′	2591
p73DBD	20	0	5′- G G G C A•T G C C C G G G C A•T G C C C -3′	2387
p73DBD	21	1	5′- G G G C A•T G C C C G G G C A•T G C C C -3′	2825
p73DBD	22	2	5′- G G G C A•T G C C C G C G G G C A•T G C C C -3′	2707
p73DBD	24	4	5′- G G G C A•T G C C C G C G C G G G C A•T G C C C -3′	2843
ΔNp73δ	20	0	5′- G G G C A•T G C C C G G G C A•T G C C C -3′	47
ΔNp73δ	21	1	5′- G G G C A•T G C C C G G G C A•T G C C C -3′	121
ΔNp73δ	22	2	5′- G G G C A•T G C C C G C G G G C A•T G C C C -3′	158
ΔNp73δ	24	4	5′- G G G C A•T G C C C G C G C G G G C A•T G C C C -3′	147

Fig. 3. Oligomerization of p73 DBD and DNA binding by p73 DBD. (*A*) Sedimentation coefficient distribution of the oligomeric species free p73 DBD and in complex with DNA containing one (12 and 14 bp) or two half-sites (20 and 24 bp). (*B*) Binding affinity constants of p73 DBD for the three half-site REs used in crystallization and of p73 DBD and ΔNp73δ for full-site REs with 0-, 1-, 2-, and 4-bp spacers. (*C*) Crystal structure of monomer A in crystal 1 in complex with DNA showing half-site RE and the residues that contact the DNA bases and the phosphate backbone. (*D*) Schematic diagram of the atomic interactions between the p73 DBD and DNA.

present a 0-bp spacer (Fig. 4*A*); in less conserved motifs, the spacer length distribution is broader (Fig. 4*B*).

To investigate the effect of RE sequence and spacer length on p73 transactivation potential, we used a yeast-based functional assay (28). In the assay, p73 REs are used as upstream enhancers of the expression of a firefly luciferase gene controlled by a minimal promoter and cloned into a constant chromosomal location in isogenic yeast strains that naturally do not contain a p73 homolog (13). In experiments with yeast cells, we previously demonstrated that human p73β protein can act as a transcription factor using constitutive and inducible promoters (29). Hence, we tested the ability of human p73β to induce the expression of the luciferase gene under the enhancer control of 10 REs with spacers from 0 to 4 bp that are variations of the three half-site sequences used for crystallization (Fig. 4*C*). The three 0-bp spacer consensus sequences examined showed that p73 was active as a transcription factor and revealed a different transactivation potential for each (C2-SP0 > C3-SP0 ≥ C1-SP0) (Fig. 4 *D* and *E*). The C2 RE was the most responsive sequence of the three and it was the least affected by the insertion of a spacer between the half-sites. In the context of promoters that produce moderate (*ADH1*) or high (*GAL1-10*) levels of p73β expression, the C2 RE with 1-bp spacer (C2-SP1) retains approximately 10% of transactivation activity, whereas insertions of 2 or 4 bp (C2-SP2 and C2-SP4) reduce the transactivation response to background levels (Fig. 4 *D* and *E*). We observed a difference in the effect of spacers on the transactivation response of p73 and p53 for the sequence C2. Whereas p73 transactivation activity dropped significantly with any insertion, p53 tolerated 1-, 2-, and 4-bp spacers without a substantial drop in activity, especially at moderate levels of expression with the constitutive *ADH1* promoter or at high levels with the *GAL1-10* promoter (Fig. 4 *F* and *G*). For REs with C1 and C3 sequences, both p73 and p53 show similar transactivation activity without spacer, but the presence of a spacer destroys activity, except for p53 with the C3-SP2 sequence that maintain some activity. In general, the presence of spacers decreases transactivation activity and it drops more rapidly for p73 than for p53.

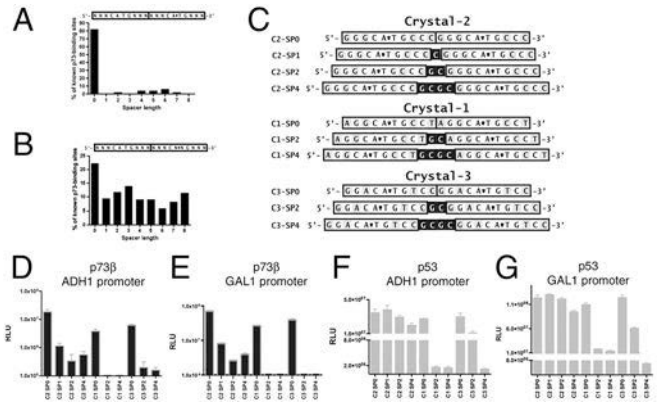

Fig. 4. Role of RE spacers in p73 transactivation. (*A* and *B*) Spacer length distribution of the 50 p73 REs reported in the p53FamTaG database with conserved central CATG bases and the 163 p73 REs reported with conserved central CATG bases in one half-site and another half-site with variable CNNG central bases. (*C*) Sequences used as enhancer of the firefly luciferase reporter gene in isogenic yeast reporter strains. The nomenclature for each RE sequence refers to the crystal form (C1, C2, or C3) and the spacer length (-SP0, -SP1, -SP2 or -SP4, in black). (*D* and *E*) Effect of sequence and spacer on p73-dependent transactivation as measured in a yeast-based functional assay. Data represent the average and standard error of four luciferase-activity assays measured for strains named in *C* at moderate levels of human p73β expression under the control of the constitutive ADH1 promoter and in *E* at high levels of expression under the inducible *GAL1-10* promoter with 0.12% galactose. The average relative-light-units (RLU) were normalized by cell-number as measured with OD at 600 nm and the zero level was defined by the basal activity with an empty expression vector. (*F* and *G*) Same as *D* and *E* for p53.

p73 DBD Quaternary Structure Depends on RE Spacer Length. Besides the described protein-DNA contacts that are identical for each monomer, in order to understand the effect of RE spacer length on p73 DBD quaternary structure, one must describe the changes in dimerization, tetramerization, and DNA conformation that occur as the number of bases between the two RE halves increases (Fig. 5). Regarding protein–protein interfaces, p73 DBD tetramers have five interaction surfaces: two are monomer–monomer surface areas that stabilize the dimers (A–B and C–D) and the other three surfaces are dimer–dimer surface contacts that form the tetramer (A–D, B–C, and B–D) (Fig. S6*A*). As spacer length

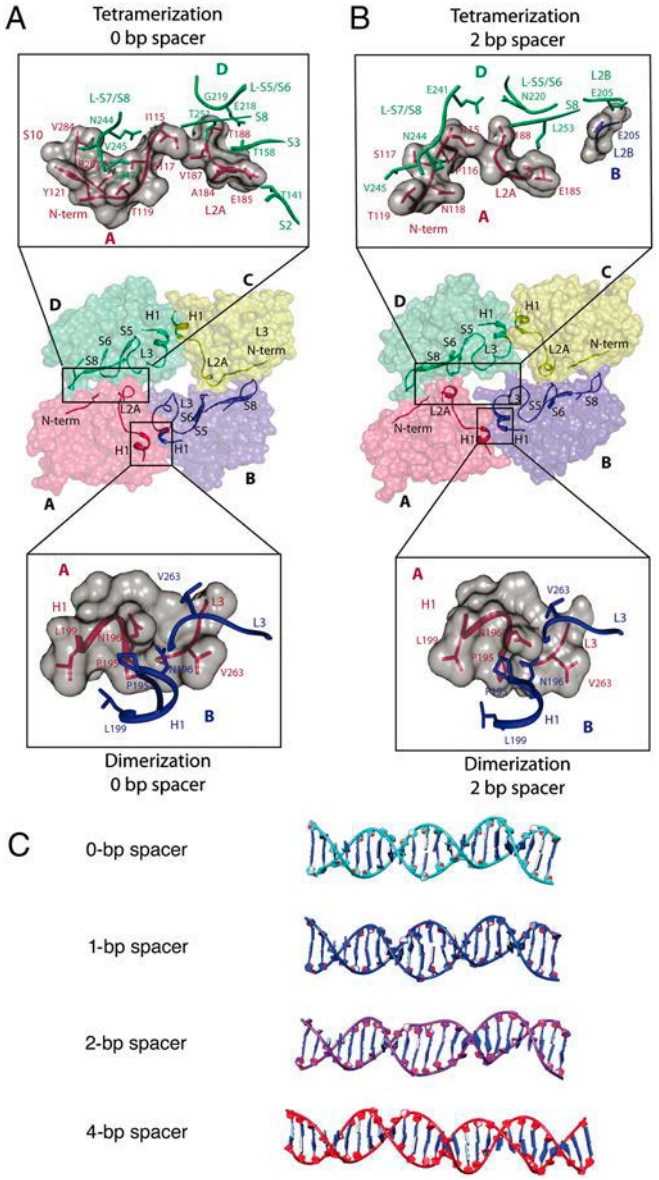

Fig. 5. Protein and DNA conformational changes on p73 DBD tetramers bound to REs with different spacers. (*A* and *B*) Dimerization and tetramerization interfaces of 0 and 2 bp tetramers. In the center of the panel, we show the secondary structure elements involved in the dimerization and tetramerization interfaces of the p73 DBD tetramer. On the top and bottom panels, we show the atomic details of the amino acids forming the tetramerization and dimerization interfaces, respectively. (*C*) DNA conformation of the refined continuous DNA molecules. The 0- and 4-bp structures conserve a B-DNA conformation, whereas the 1- and 2-bp structures twist the spacer nucleotides to unwind the double helix and allow the tetramer to continue binding to the central CATG recognition sites. Extra crystallographic refinement cycles were carried out after joining the ends of the stacked half-site RE oligonucleotides used in crystallization.

increases, the dimer–dimer distances increase and the buried surface area in the tetramer decreases (*SI Text* and Fig. S6*B*).

As observed in the sedimentation velocity experiments, a dimer is the minimum oligomer required for p73 DBD to bind to DNA (Fig. 3*A*). In all the solved structures, the dimerization interfaces are the least affected by the insertion of spacers. Nonetheless, two distinct dimer conformations could be observed (Fig. 5 and Fig. S7). One dimer conformation is influenced by tetramerization, like all the dimers in the 0- and 1-bp structures, plus the LK dimer in the 2-bp structures. The other dimer conformation represents p73 DBD dimer conformation when tetramerization restraints are weaker or absent, such as in the second IJ dimer of the 2-bp structures and the dimers of the 4-bp structure. The dimerization interface is able to establish two different hydrogen-bond networks that appear to correspond to dimers in tetramers and dimers in the absence of tight tetramerization (Fig. 5 *A* and *B*).

Tetramerization interfaces are more sensitive than the dimerization surfaces to conformational arrangement. For every base pair inserted between RE half-sites, a dimer would be expected to rotate 36° with respect to the other dimer and the distance between dimers would increase by 3.4 Å; nonetheless, the structures here described indicate that, in the presence of 1- and 2-bp spacer insertions, the forces keeping the tetramer together differ from the ideal B-DNA conformation. The dimer–dimer distance in the structures with 0- and 1-bp spacers barely increases from 34 to 35 Å (Fig. S6*B*). Instead, in the 2-bp spacer structure, one of the tetramerization interfaces is weakened; consequently, the monomer to monomer distance increases to 40 Å, and, in the 4-bp spacer structure, there is no tetramerization interface due to the 52 Å that separates two dimers. Regarding the rotation angle between dimers, the 0- and 1-bp tetramers maintain a flat dimer-of-dimers structure (Fig. S8). In contrast, with a 2-bp spacer, the p73 DBD tetramer does not maintain intact the tetramerization interface because dimers move apart 6 Å and rotate 14° out-of-plane (instead of the expected 7 Å and 72° for a 2-bp insertion) (Figs. S6 and S8). In the 2-bp spacer structure, the tetramer is not flat and, whereas one of the two tetramerization interfaces has a large 405 $Å^2$ buried surface area that is similar to the one found for 0 and 1 bp tetramers, the other tetramerization interface is disrupted and has a smaller 282 $Å^2$ buried surface (Fig. S6*B*). The tetramerization interfaces are formed by hydrogen-bond contacts and a majority of hydrophobic interactions from residues, mainly, located in the loops of the monomers (Fig. 5 *A* and *B*). As the tetramerization surface area decreases, the number of total hydrogen bonds and hydrophobic contacts in the tetramerization interface also decreases as the spacer length increases and the residues forming the tetramerization interface change, particularly loop L2A (Fig. 5 and *SI Text*).

DNA Conformation upon Tetramer Binding Depends on RE Spacer Length. Besides the described changes in the protein conformation of the p73 DBD tetramer, the conformation of the continuous DNA density that forms the full REs in the three crystal forms changes depending on the length of the RE spacer (Fig. 5*C* and Fig. S3). The DNA structure of the 0- and 4-bp spacer can be described as the classical B-DNA form; the only deviation is that the 4-bp spacer structure has a 3-Å slide in the middle of the spacer (Fig. S4 *A* and *E*). In comparison, the DNA structure in the 1- and 2-bp spacer structures show an unwinding of the DNA helix in the middle of the spacer (Fig. S4 *B–D*). A B-DNA conformation has a 36° twist at every step of the helix, but the 0- and 1-bp spacer structures show a 2° and −30° twist at the center of the RE spacer (Fig. 5*C*). Besides DNA unwinding, a slight bending toward the major groove in the same region allows to fit an extra base in the 1-bp spacer structure without distorting the quaternary structure of the tetramer. The DNA in the 2-bp spacer structure also bends slightly, but clearly not enough to compensate the extra 7 Å required to accommodate two extra base pairs without distorting the quaternary structure of the tetramer, thus some tetramer contacts break. The double-helix unwinding is the key DNA deformation that allows the tetramer to continue forming and binding to the two half-REs in spite of the additional base pairs.

Discussion

Transcription regulation is a fundamental process that underlies the molecular mechanisms of basic cellular functions, like cell growth, division, arrest, and death. We describe the quaternary structure changes in dimerization, tetramerization, and DNA conformation when p73 DBD is bound to REs of different spacer length and we measure DNA binding and in vivo p73 transactivation activity. The present manuscript shows that the distance between half-site REs affects the p73 DBD quaternary structure that acts as a scaffold to regulate p73 transactivation activity.

All the members of the p53 family have similar RE specificity (30). This work confirms that the p53 protein family has a conserved motif for DNA recognition (15–20, 22, 23, 31) (Figs. 1 and 3). The residues from the p73 DBD that contact the DNA bases (Lys138, Cys297, and Arg300) are conserved in p53 (Lys120, Cys277, and Arg280) and p63 (Lys149, Cys308, and Arg311) (Fig. 1*A*). Arg300 recognizes the conserved cytosine in the center of the half-site RE, Lys138 recognizes purines in positions 2 and 3, and Cys297 binds to the pyrimidine in position 3 (Fig. 3*C*). The p73 DBD recognizes the three DNA sequences that we studied in the same manner.

The conservation of a DNA recognition motif in the p53 protein family does not explain the different patterns of gene expression reported for p53 and p73 (7, 8). Although there is a general overlap of the p73 and p53 consensus binding sites identified by in vitro and in vivo studies, specific differences noted by SELEX, EMSA, gene reporter assays, ChIP cloning, and ChIP-sequencing analysis suggest a broader target specificity for p73 (10, 32, 33). Target specificity in the p53 protein family may partially be explained by the spacer length found between half-sites. For p53, transactivation activity is known to be affected by the number of nucleotides inserted between the two 10-bp half-sites of the full-RE (12–14). We determined the effect of RE spacer length was more drastic on the transactivation activity of p73β than for p53 and we also noted some sequence-dependent effect (Fig. 4 *D* and *E* and Fig. S6). These results suggest that p73 activation is even more sensitive to RE sequence than what has already been observed for p53 (34).

The p73 transcriptional activation is a multistep process involving DNA binding, dimerization, tetramerization, recruitment of transcriptional machinery, transcription initiation, and elongation. This study suggests that the mechanism of p73 transactivation is dependent on structural changes that occur in the oligomerization interfaces of p73 DBD tetramer upon binding to different REs. Although our structural results were obtained for p73 DBD and our transactivation results were obtained with full-length p73β, we looked for structure–function correlations that could provide some insight into how the quaternary structure of the p73 DBD–DNA complex promotes transcriptional activation. As our binding results with the ΔNp73δ isoform show, and has also been shown for p53 multidomain constructs, any effort to explain transactivation by only understanding DNA binding by the DBD is an oversimplification (22). Nevertheless, it is interesting to notice that p73 DBD quaternary structure changes correlate with the level of p73 transactivation ability. The p73 DBD tetramer bound to 0- or 1-bp spacer REs is a flat tetramer, and their transactivation activity is higher than the distorted tetramer bound to a 2-bp spacer RE, that has, if any, only basal transactivation activity.

Binding to DNA determines oligomerization and activation. Hydrodynamic experiments indicate that, in the absence of DNA, the purified p73 DBD is a monomer; then, as soon as

DNA is present, p73 DBD first dimerizes on the DNA and, if a second half-site is available, it forms a tetramer (Fig. 3*A*). REs with 2-bp spacers or shorter allow the formation of tetramers, as in crystal forms 1 and 2 or in reported structures of p53 and p63 (17–23). When p73 DBD binds to DNA with spacers larger than 2 bp, it does not form tetramers and the inability to tetramerize might explain the lack of p73β transactivation observed in the yeast-based assay. Regarding the DNA conformation, some studies on p53 have shown DNA bending (17, 18, 20), whereas others have not (19, 21, 23). In the case of p73 DBDs, dimers bind to an undisturbed B-DNA half-site RE and bending in the half-sites is not observed; on the other hand, when two oligonucleotides stack to form the 20-bp RE with 1- or 2-bp spacers, the p73 DBD tetramer is still able to recognize both half-site REs and compensates the insertions by unwinding the DNA 30° and 60°, respectively (Fig. 5*C* and Figs. S3 and S4).

Interestingly, p53 DBD binding affinity for DNA is 20 to 100 times greater than for p73 and p63 DBDs, and only our results with the ΔNp73δ isoform approach such values (22, 35) (Fig. 3*B*). The difference in affinity cannot be explained by how DNA is recognized, but it may be due to the differences in the oligomerization interfaces that have less than 50% of residues conserved between p73 and p53 (Fig. 1). The dimerization and tetramerization interfaces for the p73 DBD are smaller than for the p53 DBD. The p53 DBD dimer is held by van der Waals interactions from Pro177, His178, Met243, and Gly244 and an intermolecular salt bridge between Glu180 from the L2 loop of one monomer with Arg181 from the other monomer (20). Instead, the salt bridge is missing in p73 because Leu199 substitutes the Arg181 found in p53 and the replacement of the Met243 seen in p53 for Val263 in p73 explains the smaller interaction surface (Fig. 5*A*).

Although we have described changes in the quaternary structure of p73 DBD upon DNA binding that correlate with the transactivation activity of the full-length protein (Fig. 5), how the described active p73 DBD tetramer conformation affects the transactivation activity of the full-length protein needs to be understood.

Methods

A detailed description of the methods is available in the *SI Text*. Human p73 DBD domain (residues 115–312) was expressed in *Escherichia coli* and purified to homogeneity. Commercial DNA was lyophilized and dissolved in water to a final concentration of approximately 7 mg mL^{-1}. For crystallization trails, a molar ratio of 4:1 (protein:DNA) was used. The best crystallization conditions were 100 mM MES pH 6.0, 0.1 M ammonium acetate, and 12% (wt/vol) PEG 20000. Data were collected at beamline BL7-1 at Stanford Synchrotron Radiation Lightsource, structures were solved by molecular replacement and refined to reach low R-free values. Transactivation assays were carried out in yeast strains carrying a luciferase reporter gene. Sedimentation coefficients were measured in a Beckman Optima XL-I ultracentrifuge and DNA-binding constants were measured using 5′-fluorescein-labeled dsDNA in a Hitachi F-2000 fluorescence spectrophotometer.

ACKNOWLEDGMENTS. We thank Cristina Capitao and Tracy Truong for help during the initial stages of the project. We also thank Profs. Gourisankar Ghosh and Ulrich Mueller for critical reading of the manuscript. H.V. acknowledges the Hellman Foundation, University of California Senate, and the American Cancer Society/Internal Research Grant for generous funding. Work partially supported by the Italian Association for Cancer Research (Associazione Italiana per la Ricerca sul Cancro) IG#9086 (to A.I.) and IG#5506 (to G.F.). Diffraction data were collected at BL7-1 of the Stanford/Stanford Synchrotron Radiation Lightsource supported by the Department of Energy and National Institutes of Health (P41RR001209).

1. Kaghad M, et al. (1997) Monoallelically expressed gene related to p53 at 1p36, a region frequently deleted in neuroblastoma and other human cancers. *Cell* 90:809–819.
2. Pozniak CD, et al. (2000) An anti-apoptotic role for the p53 family member, p73, during developmental neuron death. *Science* 289:304–306.
3. Melino G, De Laurenzi V, Vousden KH (2002) p73: Friend or foe in tumorigenesis. *Nat Rev Cancer* 2:605–615.
4. Flores ER, et al. (2002) p63 and p73 are required for p53-dependent apoptosis in response to DNA damage. *Nature* 416:560–564.
5. Flores ER, et al. (2005) Tumor predisposition in mice mutant for p63 and p73: Evidence for broader tumor suppressor functions for the p53 family. *Cancer Cell* 7:363–373.
6. Murray-Zmijewski F, Lane DP, Bourdon J-C (2006) p53/p63/p73 isoforms: An orchestra of isoforms to harmonise cell differentiation and response to stress. *Cell Death Differ* 13:962–972.
7. Harms K, Nozell S, Chen X (2004) The common and distinct target genes of the p53 family transcription factors. *Cell Mol Life Sci* 61:822–842.
8. Osada M, et al. (2006) A novel response element confers p63-and p73-specific activation of the WNT4 promoter. *Biochem Biophys Res Commun* 339:1120–1128.
9. Lin Y-L, et al. (2009) p63 and p73 transcriptionally regulate genes involved in DNA repair. *PLoS Genet* 5:e1000680.
10. Smeenk L, et al. (2008) Characterization of genome-wide p53-binding sites upon stress response. *Nucleic Acids Res* 36:3639–3654.
11. Lokshin M, Li Y, Gaiddon C, Prives C (2007) p53 and p73 display common and distinct requirements for sequence specific binding to DNA. *Nucleic Acids Res* 35:340–352.
12. Riley T, Sontag E, Chen P, Levine A (2008) Transcriptional control of human p53-regulated genes. *Nat Rev Mol Cell Biol* 9:402–412.
13. Jordan JJ, et al. (2008) Noncanonical DNA motifs as transactivation targets by wild type and mutant p53. *PLoS Genet* 4:e1000104.
14. Sasaki Y, et al. (2003) Identification of the interleukin 4 receptor alpha gene as a direct target for p73. *Cancer Res* 63:8145–8152.
15. Cho Y, Gorina S, Jeffrey PD, Pavletich NP (1994) Crystal structure of a p53 tumor suppressor-DNA complex: Understanding tumorigenic mutations. *Science* 265:346–355.
16. Ho WC, Fitzgerald MX, Marmorstein R (2006) Structure of the p53 core domain dimer bound to DNA. *J Biol Chem* 281:20494–20502.
17. Kitayner M, et al. (2006) Structural basis of DNA recognition by p53 tetramers. *Mol Cell* 22:741–753.
18. Malecka KA, Ho WC, Marmorstein R (2009) Crystal structure of a p53 core tetramer bound to DNA. *Oncogene* 28:325–333.
19. Chen Y, Dey R, Chen L (2010) Crystal structure of the p53 core domain bound to a full consensus site as a self-assembled tetramer. *Structure* 18:246–256.
20. Kitayner M, et al. (2010) Diversity in DNA recognition by p53 revealed by crystal structures with Hoogsteen base pairs. *Nat Struct Mol Biol* 17:423–429.
21. Petty TJ, et al. (2011) An induced fit mechanism regulates p53 DNA binding kinetics to confer sequence specificity. *EMBO J* 30:2167–2176.
22. Chen C, Gorlatova N, Kelman Z, Herzberg O (2011) Structures of p63 DNA binding domain in complexes with half-site and with spacer-containing full response elements. *Proc Natl Acad Sci USA* 108:6456–6461.
23. Emamzadah S, Tropia L, Halazonetis TD (2011) Crystal structure of a multidomain human p53 tetramer bound to the natural CDKN1A (p21) p53-response element. *Mol Cancer Res* 9:1493–1499.
24. Menendez D, Inga A, Resnick MA (2009) The expanding universe of p53 targets. *Nat Rev Cancer* 9:724–737.
25. Weinberg RL, Veprintsev DB, Fersht AR (2004) Cooperative binding of tetrameric p53 to DNA. *J Mol Biol* 341:1145–1159.
26. Fontemaggi G, et al. (2002) Identification of direct p73 target genes combining DNA microarray and chromatin immunoprecipitation analyses. *J Biol Chem* 277:43359–43368.
27. Sbisà E, et al. (2007) p53FamTaG: A database resource of human p53, p63 and p73 direct target genes combining in silico prediction and microarray data. *BMC Bioinformatics* 8(Suppl 1):S20.
28. Andreotti V, et al. (2011) p53 transactivation and the impact of mutations, cofactors and small molecules using a simplified yeast-based screening system. *PLoS ONE* 6: e20643.
29. Monti P, et al. (2003) Characterization of the p53 mutants ability to inhibit p73 beta transactivation using a yeast-based functional assay. *Oncogene* 22:5252–5260.
30. Brandt T, Petrovich M, Joerger AC, Veprintsev DB (2009) Conservation of DNA-binding specificity and oligomerisation properties within the p53 family. *BMC Genomics* 10:628.
31. Zhao K, Chai X, Johnston K, Clements A, Marmorstein R (2001) Crystal structure of the mouse p53 core DNA-binding domain at 2.7 A resolution. *J Biol Chem* 276:12120–12127.
32. Koeppel M, et al. (2011) Crosstalk between c-Jun and TAp73{alpha}/{beta} contributes to the apoptosis-survival balance. *Nucleic Acids Res* 39:6069–6085.
33. Rosenbluth JM, Mays DJ, Jiang A, Shyr Y, Pietenpol JA (2011) Differential regulation of the p73 cistrome by mammalian target of rapamycin reveals transcriptional programs of mesenchymal differentiation and tumorigenesis. *Proc Natl Acad Sci USA* 108:2076–2081.
34. Jegga AG, Inga A, Menendez D, Aronow BJ, Resnick MA (2008) Functional evolution of the p53 regulatory network through its target response elements. *Proc Natl Acad Sci USA* 105:944–949.
35. Nikolova PV, Henckel J, Lane DP, Fersht AR (1998) Semirational design of active tumor suppressor p53 DNA binding domain with enhanced stability. *Proc Natl Acad Sci USA* 95:14675–14680.

Supporting Information

Ethayathulla et al. 10.1073/pnas.1115463109

SI Results.

The quaternary structure of the p73 DNA-binding domain (DBD) depends on the spacer length of the response element (RE). The dimerization interface between two monomers binding to half-RE is the interface less affected by changes in spacer length. As seen in the sedimentation velocity experiments, a dimer is required for p73 DBD to bind to DNA. The p73 DBD dimers bound to a 4-bp spacer in crystal 3, where there is no dimer–dimer contacts, probably best represent how p73 DBD binds to DNA as a dimer (Fig. 2*D*), whereas the conformation of the eight unique dimers from crystal forms 1 and 2 are somehow affected by dimer–dimer contacts. The average distance between the monomers across the dimerization interface, as defined by a centroid of each monomer in the dimer, is always 44 Å and all the solved structures have a similar buried surface area of between 209 and 226 $Å^2$; both measurements remain almost unchanged, even if the spacer length increases (Fig. S6). In spite of the dimer similarity, a noticeable rearrangement of the dimerization angle is observed when the 11 unique dimers contained in the three crystal structures solved are compared (Fig. S7). Two main dimer conformations are seen when dimers of the 0- and 1-bp spacer structures are compared with the dimers of the 4-bp spacer structure. For the 2-bp spacer structure, one dimer resembles the short spacer conformation, whereas the second dimer resembles the long spacer conformation. For dimers that contact other dimers to create a tetramerization surface, the dimerization interface is stabilized by hydrogen bonds between the Oδ1 and Nδ2 from Asn196 in the α-helix H1 of one monomer and Asn196 Nδ2 and Val263 O in the L3 from the other monomer (Fig. 5*A*). In the case of dimers with a reduced tetramerization surface or completely absent, the hydrogen bond between Asn196 Nδ2 and Val263 O breaks allowing the dimerization interface to rotate (Fig. 5*B*). In both cases, Pro195, Leu199, and Val263 from both monomers contribute with hydrophobic and van der Waals interactions to form the dimerization surface. In conclusion, the dimerization interface is able to establish two different hydrogen-bond networks that appear to correspond to active and inactive p73 DBD tetramers.

The dimerization interfaces are less sensitive than tetramerization surfaces to conformational arrangement as spacer length increases (Fig. S6*B*). It would be expected that, for every base pair inserted between the half-site REs, a dimer would need to rotate 36° with respect to the other dimer and the distance between them would increase by 3.4 Å; nonetheless, the structures here described indicate that, in the presence of 1- and 2-bp spacer insertions, the forces keeping the tetramer together deviate the DNA conformation from the ideal B-DNA form. The dimer–dimer distance, measured as the C^{α}–C^{α} distance between two Arg300 residues across the tetramerization interface is almost identical, 34 versus 35 Å, for the tetramers with 0- and 1-bp spacers (Fig. S6*B*). Instead, in the 2-bp spacer structure, one of the tetramerization interfaces is weakened; consequently, the monomer-to-monomer distance increases to 40 Å. In the 4-bp spacer structure, there is no tetramerization interface due to the 52 Å that separate two dimers (Fig. S6*B*). Regarding the rotation angle between dimers, the 0 and 1 bp tetramers maintain a flat dimer-of-dimers structure (Fig. S8). Interestingly, although the buried surface area between both 0 and 1 bp tetramers is between 440 and 470 $Å^2$, the total number of atoms forming the tetramerization interfaces in the 0-bp spacer structure is considerably larger (113 atoms) than in the 1-bp spacer structure (66 atoms) (Fig. S6*B*). This significant difference is because the extra base pair in the 1-bp spacer structure separates the atoms in the tetramerization interface by 1 Å, but the tetramer remains flat with the same solvent inaccessible surface area and it does not rotate 36° as expected from having a 1-bp insertion. In contrast, with a 2-bp spacer, the p73 DBD tetramer cannot maintain intact the integrity of the tetramerization interface because dimers move 6 Å and rotate 14° out-of-plane (instead of the expected 7 Å and 72° for a 2-bp insertion) (Fig. S8). In the 2-bp spacer structure, the tetramer is not flat and, whereas one of the two tetramerization interfaces has a large 405 $Å^2$ buried surface area that is similar to the one found for 0 and 1 bp tetramers, the other tetramerization interface is disrupted and has a smaller 282 $Å^2$ buried surface (Fig. S6*B*). The tetramerization interface does not form in the case of the structure with a 4-bp spacer.

As the tetramerization surface area decreases, the number of total hydrogen bonds and hydrophobic contacts in the tetramerization interface also decreases as the spacer length increases. The 0-, 1-, and 2-bp spacer tetramerization interfaces have a total of 14, 10, and 6 hydrogen bonds, respectively. In the 0- and 1-bp spacer structures, the A–D and B–C interfaces are formed by the interaction between two patches of contacts with residues in the N-terminal, L2A, S10 from monomer A or C, and residues in L1, S8, and three small loops between S2′–S3, S5–S6, and S7–S8 from monomer B or D (Figs. 1*A* and 5*A*). One network involves a surface formed by residues Ile115, Pro116, Ser117, and Thr119 from the N-terminal in monomer A and Val284 and Arg287 from β-strand S10 with a complementary surface formed by Gln244, Val245, and Thr247 in the loop between S7–S8 in monomer D. The second hydrogen-bonding network involves residues Ala184, Glu185, Val187, and Thr188 in loop L2A of monomer A with residues Thr141, Thr158, Glu218, Gly219, and Thr251 in monomer D. In the 2-bp spacer structure, the monomer–monomer B–C interface is formed by the same secondary elements as in the active tetramers and it has a buried surface of 405 $Å^2$, close to the 440–470 $Å^2$ of the active tetramers. In contrast, the buried solvent accessible surface area of the second A–D tetramerization interface is only 282 $Å^2$. The larger 2-bp spacer shifts out monomer D from the center of the tetramer, creating a smaller interaction surface, preventing strand S10 from monomer A and loops L1 and S2–S3′ in monomer D from being part of the interface (Figs. 1*A* and 5*B*). Such changes result in a tetramerization interaction only present in the 2-bp structures between Glu205 in the L2 loops of monomers B and D (Fig. 5*B*).

In the p73 tetramers bound to 0- or 1-bp spacer REs, loop L2A is the key secondary structure element from monomers A and C that makes the most extensive contacts with the adjacent monomers B and D keeping the tetramer flat. Loop L2A contacts residues in S2, S3, S8, and L-S5/S6 allowing the N terminus to establish a large tetramerization surface (Fig. 5*A*). Moreover, the movement of L2A toward the interacting dimer moves H1, decreasing the dimerization angle in the monomer–monomer interface, resulting in distinct dimerization interfaces for the structures of 0- and 1-bp spacers than for structures with larger spacers (Fig. S7). In the tetramer bound to a 2-bp spacer RE, the number of contacts between monomer A and monomer D decrease substantially and L2A is no longer able to change the angle of dimerization between monomer A and monomer B (Fig. 5*B*). Even if one of the tetramerization surfaces in the 2-bp spacer tetramer is interrupted, the second tetramerization interface regains the contacts observed in the dimers and tetramers bound to 0- or 1-bp spacer REs. The rearrangement of the dimerization and

tetramerization interfaces upon binding to different REs appear to correlate with p73 transactivation capability.

SI Methods.

Protein Expression and Purification. The human p73 DBD (residues 115–312) was cloned into the pET28(a) bacterial expression vector with a His-tag in the N terminus. BL21/DE-3 *Escherichia coli* cells were transformed with the plasmid and grown in LB medium at 37 °C. When cultures reached an absorbance 0.6 AU at 600 nm, cells were induced with 0.5 mM IPTG and grown at 25 °C for 4 h. Cells were harvested by centrifugation at $3,500 \times g$ and resuspended in lysis buffer [20 mm sodium citrate (pH 6.1), 500 mM NaCl, 10 μm $ZnCl_2$]. Cells were lysed using a French press and cellular debris was removed by centrifugation at $25,000 \times g$. Protein was first affinity-purified by adding 1 mL Ni-nitrilotriacetate resin to the supernatant containing soluble p73 DBD and kept stirring for 1 h at 4 °C for batch binding. The protein bound resin was washed with abundant lysis buffer and eluted with buffer containing 200 mM imidazole [20 mM sodium citrate (pH 6.1), 500 mM NaCl, 10 μm $ZnCl_2$, and 200 mM imidazole]. The eluted protein was concentrated and further purified by size-exclusion chromatography using Superdex200 16/60 in a low-salt buffer [10 mm sodium citrate (pH 6.1), 100 mM NaCl, 5 μm $ZnCl_2$, and 5 mM DTT]. Peak fractions were collected and concentrated to 20 mg/mL. Purity was assessed by SDS-PAGE and MALDI-TOF. Oligonucleotides with sequences 5′-CAGGCATGCCTG-3′ (12 bp), 5′-CGGGCATGCCCG-3′ (12 bp), and 5′-ATGGACATGTCCAT-3′ (14 bp) were acquired commercially (ValueGene), lyophilized, and dissolved in water to obtain a final concentration of 7 and 6.8 mg mL^{-1}.

Crystallization. For crystallization trials, a molar ratio of 4 : 1 (protein:DNA) between p73 DBD (20 mg mL^{-1}) and DNA were used. A hanging-drop vapor diffusion method was used at 23 °C. Each drop contained 1 μL protein-DNA solution and 1 μL reservoir solution equilibrated against 0.5 mL reservoir solution. The best crystals were obtained for crystals 1 (5′-CAGGCATGCCTG-3′) and 2 (5′-CGGGCATGCCCG-3′) in 100 mM MES (pH 6.0), 0.1 M ammonium acetate, and 12% (wt/vol) PEG 20000 and for crystal 3 (5′-ATGGACATGTCCAT-3′) in 100 mM MES (pH 6.5), 0.1 M ammonium acetate, and 12% (wt/vol) PEG 20000. Crystals were frozen using reservoir buffer with 10% glycerol as cryoprotectant.

Data Collection and Structure Determination. Crystals 1 and 2 diffracted to 2.95-Å resolution and crystal 3 to 4-Å resolution (Table S1). Datasets were collected at beamline BL7-1 of the Stanford Synchrotron Radiation Lightsource on a MarMosaic-325 CCD detector and processed using HKL2000 (1). Crystal data and intensity statistics are given in Table S1. Crystal 1 belongs to monoclinic $P2_1$ space group with unit cell parameters $a = 82.09$ Å, $b = 104.52$ Å, $c = 122.99$ Å, $\beta = 96.18°$; crystal 2 is also monoclinic $P2_1$ space group with unit cell parameters $a = 82.54$ Å, $b = 104.20$ Å, $c = 123.22$ Å, $\beta = 96.50°$; and crystal 3 is monoclinic $C2$ space group with unit cell parameters $a = 158.40$ Å, $b = 91.12$ Å, $c = 137.47$ Å, $\beta = 90.20°$. The asymmetric unit of crystal 1 and crystal 2 consists of eight 198 amino acid p73 DBD molecules and four double-strand 12 bp DNA molecules and crystal 3 consists of six p73 DBD molecules and three double-strand 14 bp DNA molecules. The structures were solved by molecular replacement using as a search model a p53 DBD dimer (Protein Data Bank code 3KMD; ref. 2) in complex with the ideal 12 or 14 bp DNA used in crystallization. Phaser was used to find the molecular replacement solution (3). For crystal 1 and crystal 2, the molecular replacement solution yielded four unique peaks with four DBD dimers (eight monomer molecules) and four 12 bp dsDNA molecules forming two tetramers and, for crystal 3, three p73 DBD dimers (six monomer molecules) and three 14 bp dsDNA molecules forming three dimers were obtained. The solutions were refined using rigid body, simulated annealing, and energy minimization protocols as implemented in CNS v1.3 (4). Simulated annealing composite omit maps were calculated and manual building was carried out using Coot 0.6.1 (5). Iterative cycles of automatic and manual refinement were carried out. In crystal 1, the 12th base of chains E, F, G, and H are protruding outside the DNA helical axis and only two of them have defined density; in crystal 2, the 12th base of chain E and F are protruding outside the DNA helical axis; and, in crystal 3, the 14th base in chain G and H was not built due to the clash with the symmetry-related molecule. Water molecules were added toward the end of refinement. Refinement statistics are given in Table S1. The refined structures were validated by PROCHECK (6). Almost all (99.5%) of the residues of crystal 1 are in allowed or generally allowed regions of the Ramachandran plot, 99.6% for crystal 2 and 99.3% for crystal 3 (7). As a control of DNA continuity, we carried out an extra refinement step where the ends of stacking DNA molecules where joined with a phosphodiester bond as if they were a single molecule. The results of the control refinement are shown in Fig. S4.

Yeast Strains and Media. A panel of isogenic haploid strains of the yeast *Saccharomyces cerevisiae* were constructed and used to measure p53 and p73 transactivation potential. The reporter strains are based on the previously described yLFM-REs yeast strains (8) and contained the consensus sequence elements used in the crystallization studies and listed in Fig. 3*C*. For the construction of the new yLFM-REs strains, we took advantage of the Delitto perfetto approach for promoter modifications by oligonucleotide targeting (9). The haploid strain yIG397 (3XRGC::pCYC1::ADE2) was used for the gap repair assay (10). Cells were grown in 1% yeast extract, 2% peptone, 2% dextrose with the addition of 200 mg/L adenine or in selective medium (with 2% dextrose or 2% raffinose as carbon source) lacking tryptophan with the addition of adenine (200 mg/L). Galactose (0.128%) was added to the medium in order to achieve a high expression of p53 and p73 proteins under the inducible *GAL1.10* promoter.

Yeast Expression Vectors. For constitutive expression in yeast of human p53 and p73β the ADH1-based vectors pTS76 (11) and pTSp73β (present work) were used, respectively. The pTSp73β vector was constructed using a PCR-based approach followed by gap repair assay (10). The entire p73β coding sequence was amplified starting from p73βT plasmid (12) using a pair of primers that comprise homology tails (sequence in bold) for recombinational cloning in yeast (p73-N-terATG: 5'-caagctatac-caagcatacaatcaactatctcatatacagttaactcgagatggcccagtccaccgccacc-3'; p73β-CterTGA: 5'-gacataactaattacatgatggtggcggccgctctagaactagtg-gatcctcagggcccccaggtcctgacgaggctggg-3'). The homology tails contained also the target sequence of the XhoI and NotI restriction enzymes. Hence, both ends of the PCR product will be identical to the ends of an acceptor plasmid (pTS-based) that is double digested (XhoI/NotI) before being cotransformed with the PCR product in yeast cells. In yeast, the plasmid is resealed together with the PCR products by recombination, exploiting the sequence homology at the end of the fragments (gap repair assay). Plasmid DNA was recovered from yeast transformants, expanded in *E. coli*, and the correct integration of the p73β coding sequence was verified at the molecular level by restriction and DNA sequencing (BMR Genomics). Galactose inducible expression (*GAL1.10* promoter) of the human p53 and p73 proteins was achieved using the pTSG-p53 (9) and pTSG-p73β (present work) vectors. The pTSG-p73β vector was constructed starting from double digestion of pTSp73β plasmid (XhoI and NotI); the fragment corresponding to the p73β coding sequence was then cloned

in a double digested pTSG-based (*GAL1* promoter) vector by ligation. The pRS314 plasmid was used in all experiment as empty vector. All vectors contain the yeast selectable marker TRP1.

Luciferase Assays in Yeast. The panel of yLM-REs strains were transformed by the lithium acetate method with the p53 and p73 expression vectors or the empty vector used as a control for background luciferase activity. Transformants were selected on minimal plates lacking tryptophan but containing 200 mg/L adenine to allow the growth of white colonies with normal size. After 2–3 d of growth at 30 °C, transformants were streaked onto the same type of plate and allowed to grow for an additional day. The luciferase assay was conducted according to the miniaturized protocol we recently developed (13). For *ADH1*-based p53 and p73 experiments, yeast transformants were resuspended in 150 μL of water and OD_{600} was directly measured in a transparent 96-well plate. Twenty microliters of cells suspension was transferred and mixed with an equal volume of Passive Lysis Buffer buffer 2× (Promega) in a white 96-well plate. After 15 min of shaking at room temperature, 20 μL of Firefly luciferase substrate (Bright Glo; Promega) was added. Light units were normalized to optical density and the background luminescence of each reporter strain containing empty expression vector was subtracted. For the *GAL1.10*-based experiments, cells were resuspended in minimal synthetic medium containing raffinose (2%) (only for p53 experiments) or raffinose plus galactose (0.128%) in a final volume of 120 μL (96-well plate). Cells suspensions were grown for 8 h with vigorous shaking and processed as described previously (13).

Analytical Ultracentrifugation. Sedimentation velocity experiments were performed in 100 mM NaCl, 10 mM sodium citrate (pH 6.1), 5 mM DTT, 5 μM $ZnCl_2$ using Beckman Optima XL-I analytical ultracentrifuge with an AnTi-60 rotor. Four hundred microliters of 416 μM p73 DBD and 400 μL of buffer were loaded into a double-sector centerpiece. The experiment was carried out at 50,000 rpm, 20 °C, and the radial scans were collected at 280 nm. For fluorescence experiments, 400 μL of protein-DNA complex containing 64.5 μM of p73DBD and 3–3.4 μM of 5′-fluorescein-labeled dsDNA (12 bp, 5′-FAM/TGGGCATGCCCA-3′; 14 bp, 5′-FAM/ATGGGCATGCCCAT-3′; 20 bp, 5′-FAM/GGGCATGCCCGGGCATGCCC-3′; 24 bp, 5′-FAM/TCGGGCATGCCCGGGCATGCCCGA-3′) and 400 μL of buffer were loaded into double-sector centerpieces. The experiments were carried out at 50,000 rpm, 20 °C, and the radial scans were collected at 488 nm. The collected data were analyzed using SEDFIT software to calculate sedimentation coefficient distributions (14). SEDNTERP software was used to calculate the partial specific volume, buffer viscosity, and buffer density (15)

Fluorescence Polarization. The p73DBD was serially diluted in 100 mM NaCl, 10 mM sodium citrate (pH 6.1), 5 mM DTT, 5 μM $ZnCl_2$ from 100 μM to 1 nM and there were total of 17 tubes prepared with different concentrations at a final volume of 500 μL. The 5′-fluorescein-labeled dsDNA (12-mer, 5′-FAM/TGGGCATGCCCA-3′; 12-mer, 5′-FAM/CAGGCATGCCTG-3′; 14-mer, 5′-FAM/ATGGACATGTCCAT-3′; 24-mer, 5′-FAM/TCGGGCATGCCCGGGCATGCCCGA-3′; 21-mer-1sp 5′-FAM/GGGCATGCCCCGGGCATGCCC-3′; 22-mer-2sp 5′-FAM/GGGCATGCCCGCGGGCATGCCC-3′ and 24-mer-4bp 5′-FAM/GGGCATGCCCGCGCGGGCATGCCC-3′) were added into each tube to a final concentration of 5 nM. The tubes were incubated at room temperature for 45 min. The fluorescence intensity of each tube was measured using Hitachi F-2000 Fluorescence Spectrophotometer with excitation and emission wavelengths of 494 and 521 nm, respectively. The fluorescence polarization data was analyzed using nonlinear regression in graphical software Prism.

1. Otwinowski Z, Minor W (1997) Processing of X-ray diffraction data collected in oscillation mode. *Methods Enzymol* 276:307–326.
2. Chen Y, Dey R, Chen L (2010) Crystal structure of the p53 core domain bound to a full consensus site as a self-assembled tetramer. *Structure* 18:246–256.
3. McCoy AJ, et al. (2007) Phaser crystallographic software. *J Appl Crystallogr* 40(Pt 4):658–674.
4. Brunger AT (2007) Version 1.2 of the Crystallography and NMR system. *Nat Protoc* 2:2728–2733.
5. Emsley P, Cowtan K (2004) Coot: Model-building tools for molecular graphics. *Acta Crystallogr D Biol Crystallogr* 60(Pt 12 Pt 1):2126–2132.
6. Laskowski R, MacArthur M, Moss D, Thornton J (1993) PROCHECK: A program to check the stereochemical quality of protein structures. *J Appl Crystallogr* 26:283–291.
7. Ramachandran GN, Sasisekharan V (1968) Conformation of polypeptides and proteins. *Adv Protein Chem* 23:283–438.
8. Tomso DJ, et al. (2005) Functionally distinct polymorphic sequences in the human genome that are targets for p53 transactivation. *Proc Natl Acad Sci USA* 102:6431–6436.
9. Jegga AG, Inga A, Menendez D, Aronow BJ, Resnick MA (2008) Functional evolution of the p53 regulatory network through its target response elements. *Proc Natl Acad Sci USA* 105:944–949.
10. Flaman JM, et al. (1995) A simple p53 functional assay for screening cell lines, blood, and tumors. *Proc Natl Acad Sci USA* 92:3963–3967.
11. Inga A, et al. (1997) Determining mutational fingerprints at the human p53 locus with a yeast functional assay: A new tool for molecular epidemiology. *Oncogene* 14:1307–1313.
12. Monti P, et al. (2003) Characterization of the p53 mutants ability to inhibit p73 beta transactivation using a yeast-based functional assay. *Oncogene* 22:5252–5260.
13. Andreotti V, et al. (2011) p53 transactivation and the impact of mutations, cofactors and small molecules using a simplified yeast-based screening system. *PLoS ONE* 6: e20643.
14. Lebowitz J, Lewis MS, Schuck P (2002) Modern analytical ultracentrifugation in protein science: A tutorial review. *Protein Sci* 11:2067–2079.
15. Laue TM, Shan BD, Ridgeway TM, Pelletier SL (1992) Computer-aided interpretation of analytical sedimentation data for proteins in analytical ultrafugation. *Analytical Ultracentrifugation in Biochemistry and Polymer Science*, eds Horton JC, Rowe AJ (Royal Society of Chemistry, Cambridge, UK), pp 90–125.

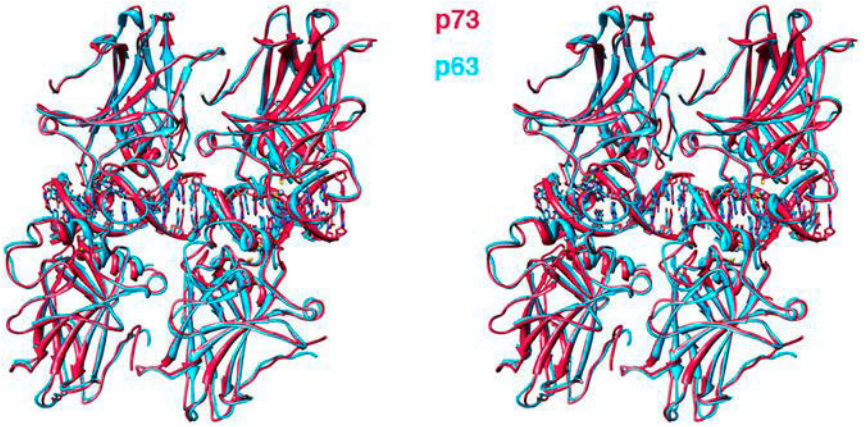

Fig. S1. Superposition of structure from crystal 1 of p73 DBD tetramer bound to a 0-bp spacer RE with structure of p63 DBD tetramer bound to DNA in type II tetramer arrangement (1).

1 Chen C, Gorlatova N, Kelman Z, Herzberg O (2011) Structures of p63 DNA binding domain in complexes with half-site and with spacer-containing full response elements. *Proc Natl Acad Sci USA* 108:6456–6461.

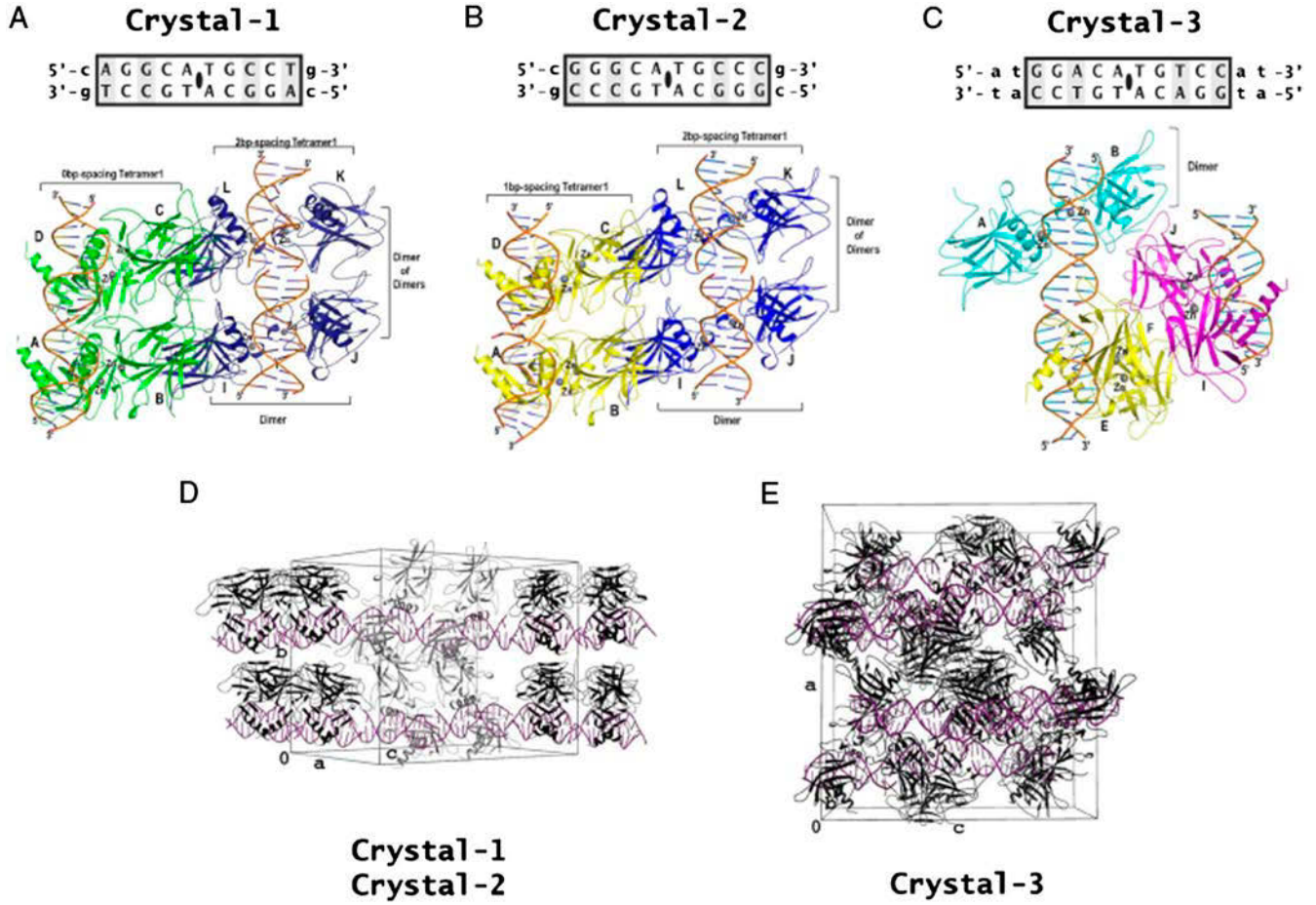

Fig. S2. Asymmetric unit and unit cell packing in the three crystals forms solved. (*A*) Packing in the asymmetric unit of crystal 1 contains two tetramers with four double-strand 12 bp oligonucleotides (5′-cAGGCATGCCTg-3′). Tetramer ABCD (green) is bound to two oligonucleotides that form a 0-bp spacer RE and the second tetramer, IJKL (blue), is bound to two oligonucleotides that form a 2-bp spacer RE. DNA molecules are shown in orange, and zinc atoms in gray. (*B*) Packing in the asymmetric unit of crystal 2 contains two tetramers with four double-strand 12 bp oligonucleotides (5′-cGGGCATGCCCg-3′). Tetramer ABCD (yellow) is bound to two oligonucleotides that form a 1-bp spacer RE and the second tetramer, IJKL (blue), is bound to two oligonucleotides that form a 2-bp spacer RE. DNA molecules are shown in orange, and zinc atoms in gray. (*C*) Packing of in the asymmetric unit of crystal 3 contains three dimers with six double-strand 14 bp oligonucleotides (5′-atGGACATGTCCat-3′). Dimers AB (cyan) and EF (yellow) are bound to two oligonucleotides that form a 4-bp spacer RE. The DNA in the third dimer JI (magenta) form a 4-bp spacer with a symmetry-related dimer. DNA molecules are shown in orange, and zinc atoms in gray. (*D*) Unit cell packing in crystals 1 and 2 is the same. Protein chains are shown in black, DNA in magenta, and the two tetramers in the asymmetric unit in gray. The view shows DNA stacking in the unit cell as a continuous double-helix. (*E*) Unit cell packing in crystal 3. Protein chains are shown in black and DNA in magenta. The view shows DNA stacking in the unit cell as a continuous double-helix.

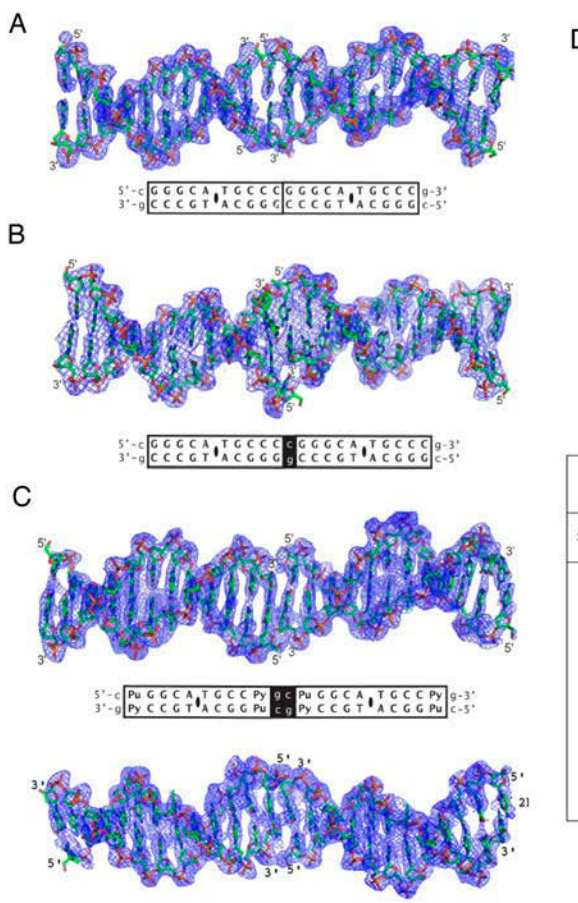

C1'-C1' Distances for the two central A-T base pairs

Ideal DNA	Kitayner et al 2010	Crystal - 1	Crystal-2	Crystal-3
5'-cGGGCATGCCCg-3'	5'-cGGGCATGCCCg-3'	5'-cAGGCATGCCTg-3'	5'-cGGGCATGCCCg-3'	5'-atGGACATGTCCat-3'
10.66 10.66 Watson-Crick	8.29 8.29 Hoogsteen	10.44 9.78 Dimer AB 10.18 10.35 Dimer CD 9.92 10.33 Dimer IJ 9.95 10.50 Dimer KL	10.54 9.91 Dimer AB 10.03 10.22 Dimer CD 10.47 9.94 Dimer IJ 9.88 10.43 Dimer KL	9.96 10.38 Dimer AB 9.85 10.16 Dimer EF 10.48 10.12 Dimer IJ

Fig. S3. DNA density. (*A*) DNA $2F_o - F_c$ composite omit map for the 0-bp spacer tetramer. The density for the 11th and 12th base pairs (TG-CA) of the crystallization oligonucleotide could not be observed. The map shows a continuous DNA stacked as shown in density map. The electron density is contoured at 1 s cutoff. (*B*) DNA $2F_o - F_c$ composite omit map for the 1-bp spacer tetramer. The 12th base pair (G–C) flip away from the DNA helical axis between the stacked DNAs. (*C*) DNA $2F_o - F_c$ composite omit map for the two 2-bp spacer tetramers, one from crystal 1 and the other from crystal 2. Two 12 bp double-strand DNA stack without flipping any base forming a continuous DNA density. (*D*) DNA $2F_o - F_c$ composite omit map for the two 4-bp spacer tetramer from crystal 3. (*E*) C1'-C1' distances for the two central A-T base pairs.

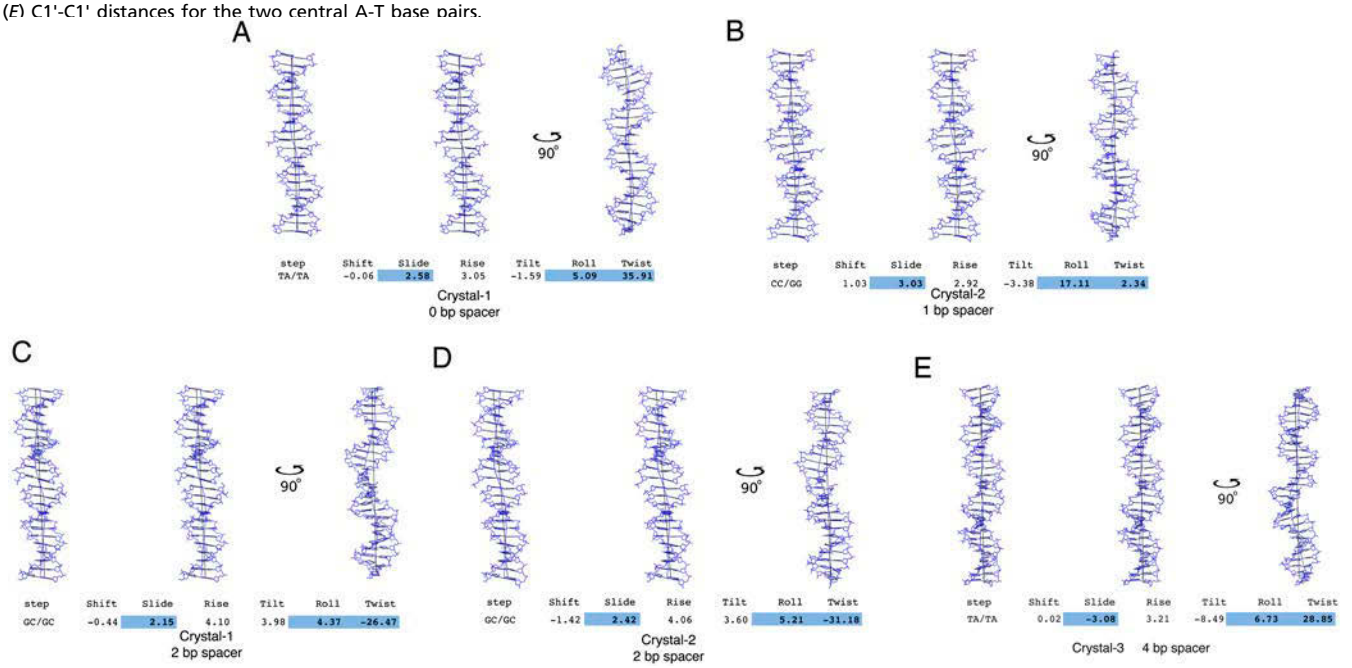

Fig. S4. DNA conformation in the structure of p73 DBD tetramer bound to REs with different spacing. (*A–E*) Global helical axis as calculated with 3DNA appears as B-DNA with a view at a 90° rotation and the local base step parameters as calculated using 3DNA for the step in the middle of the spacer of the five continuous full REs. *A* and *E* maintain B-DNA conformation, whereas *B–D* unwind the DNA and have non-B-DNA twists.

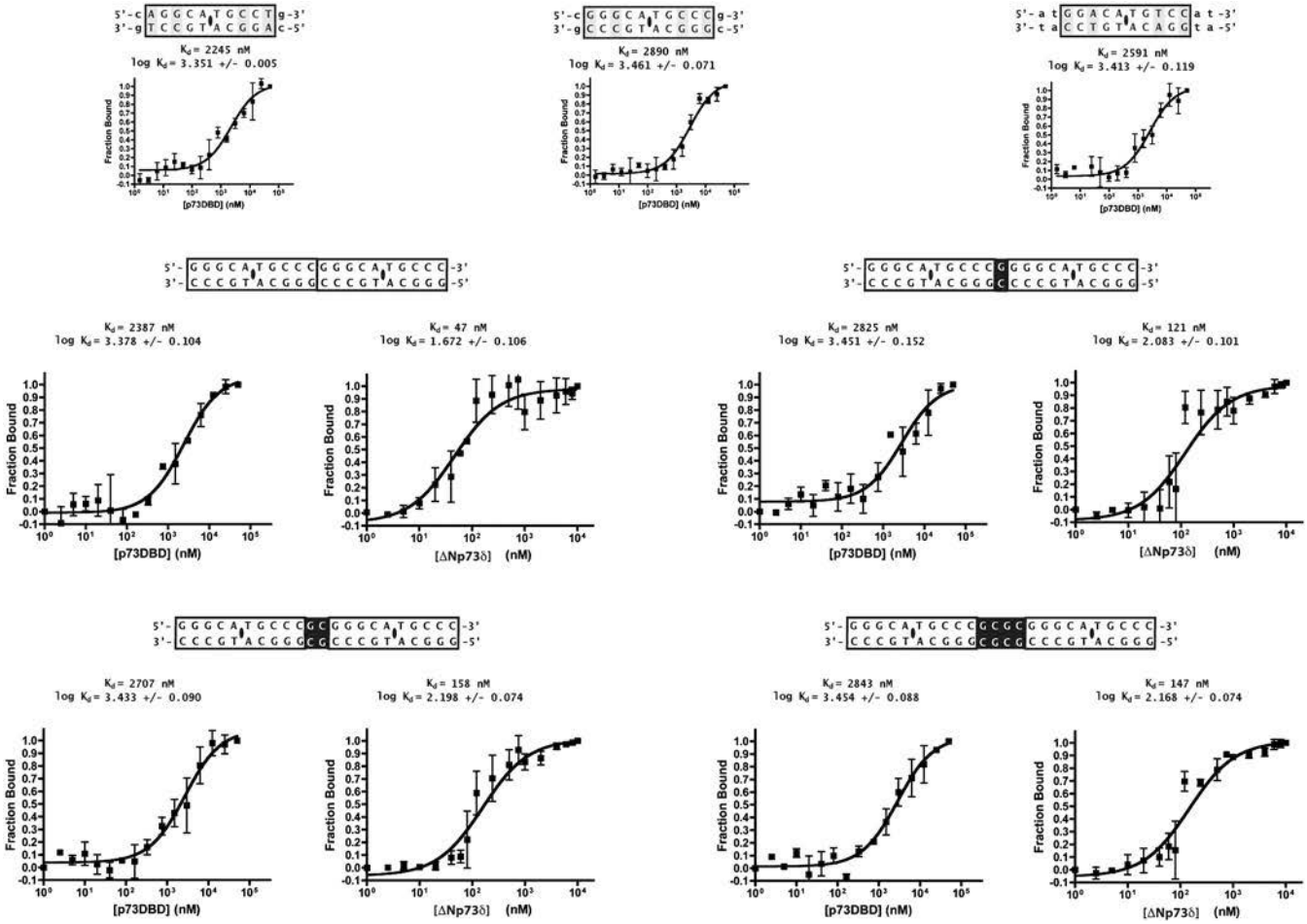

Fig. S5. Binding affinity graphs of p73 DBD for the three half-site REs used in crystallization and of p73 DBD and ΔNp73δ for full-site REs with 0-, 1-, 2-, and 4-bp spacers.

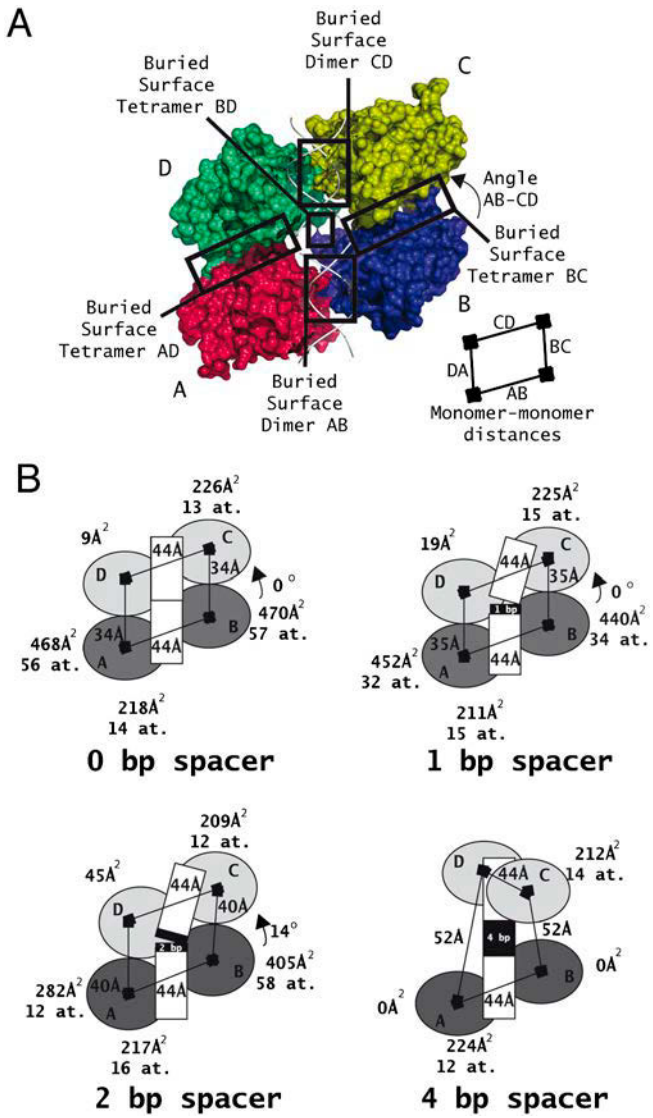

Fig. S6. Protein–protein interfaces and quaternary structure changes of p73 DBD upon DNA binding. (*A*) Surface representation of p73 DBD tetramer with a 0-bp spacer indicating the angles, distances, and surfaces of dimerization and tetramerization. There are one dimer–dimer angle of tetramerization (AB–CD), two buried surface areas of dimerization (AB and CD), three buried surface areas of tetramerization (AD, BD, and BD), and four monomer-monomer distances (AB, BC, CD, and DA). (*B*) Parameters of oligomerization described in *A* for each of the p73 DBD in complex with RE of 0, 1, 2, and 4 bp. The number of atom pairs involved in a buried surface area is below the surface area value.

A

	0bp spacer Crystal1-AB	0bp spacer Crystal1-DC	1bp spacer Crystal2-AB	1bp spacer Crystal2-DC	2bp spacer Crystal1-LK	2bp spacer Crystal2-LK	2bp spacer Crystal1-IJ	2bp spacer Crystal2-IJ	4bp spacer Crystal3-AB	4bp spacer Crystal3-DC	4bp spacer Crystal3-IJ	
Crystal1-AB (403 aa)		0.75	0.60	0.85	1.11	1.20	1.57	1.65	1.71	1.68	2.10	0bp spacer
Crystal1-DC (402 aa)	0.75		0.73	0.65	1.12	1.25	1.45	1.52	1.62	1.54	1.87	0bp spacer
Crystal2-AB (401 aa)	0.60	0.73		0.87	1.11	1.28	1.72	1.96	1.80	1.76	2.16	1bp spacer
Crystal2-DC (398 aa)	0.85	0.65	0.87		1.28	1.33	1.35	1.49	1.95	1.92	1.48	1bp spacer
Crystal1-LK (407 aa)	1.11	1.12	1.11	1.28		0.74	2.01	2.12	2.06	2.11	1.86	2bp spacer
Crystal2-LK (402 aa)	1.20	1.25	1.28	1.33	0.74		1.96	2.16	1.90	1.87	2.26	2bp spacer
Crystal1-IJ (398 aa)	1.57	1.45	1.72	1.35	2.01	1.96		0.69	1.03	1.04	1.19	2bp spacer
Crystal2-IJ (398 aa)	1.65	1.52	1.96	1.49	2.12	2.16	0.69		1.28	1.20	1.09	2bp spacer
Crystal3-AB (403 aa)	1.71	1.62	1.80	1.95	2.06	1.90	1.03	1.28		0.83	1.27	4bp spacer
Crystal3-DC (402 aa)	1.68	1.54	1.76	1.92	2.11	1.87	1.04	1.20	0.83		1.20	4bp spacer
Crystal3-IJ (399 aa)	2.10	1.87	2.16	1.48	1.86	2.26	1.19	1.09	1.27	1.20		4bp spacer

B

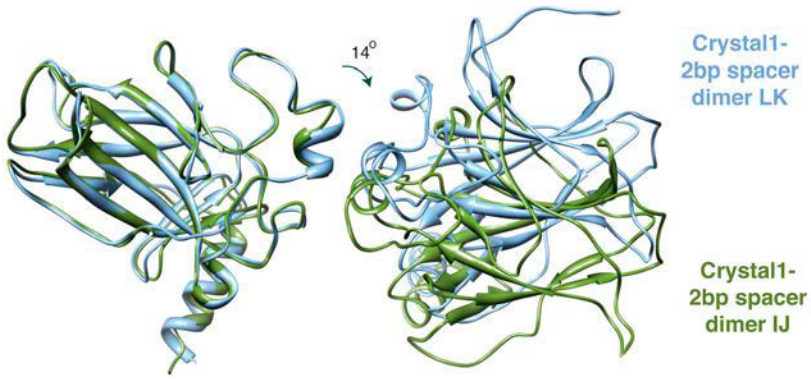

Fig. S7. Conformational change of p73 DBD dimers. (*A*) Table with the overall root-mean-square deviation of comparing two dimers. The 11 independent dimers found in the three crystal forms were superimposed. Two main conformations are found, one for the 0, 1 and LK-2 bp dimers (blue) and another for the IJ-2 bp and 4 bp dimers (green). (*B*) Two dimer conformations found. When superimposing the dimer IJ with the dimer LK of the 2 bp tetramer from crystal 1, the 15° rotation of the orientation of the dimers becomes obvious.

A

	0bp spacer Crystal1-ABCD	1bp spacer Crystal2-ABCD	2bp spacer Crystal1-IJKL	2bp spacer Crystal2-IJKL	
Crystal1-ABCD (805 aa)		0.65	2.29	2.25	0bp spacer
Crystal2-ABCD (799 aa)	0.65		2.39	2.30	1bp spacer
Crystal1-IJKL (805 aa)	2.29	2.39		0.72	2bp spacer
Crystal2-IJKL (800 aa)	2.25	2.30	0.72		2bp spacer

B

C

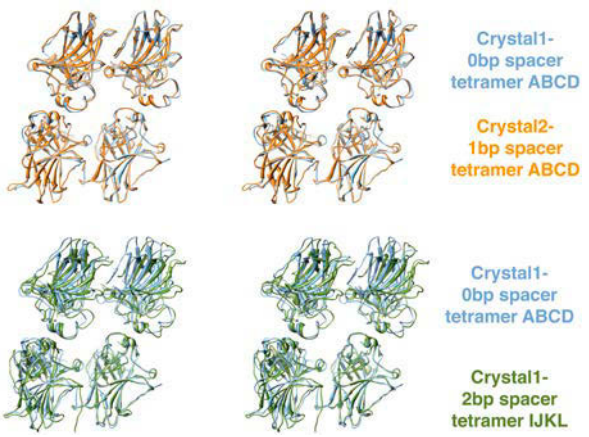

Fig. S8. Conformational change of p73 DBD tetramers. (*A*) Table with the overall root-mean-square deviation of comparing two tetramers. The four independent dimers found in crystal forms 1 and 2 were superimposed. Two main conformations are found, one for the 0 and 1 bp tetramers (blue) and another for the 2 bp tetramers (green). (*B*) Tetramers with 0- and 1-bp spacers have similar quaternary structure. When superimposing the 0 and 1 bp tetramer from crystals 1 and 2, respectively, all the monomers superimpose. (*C*) Tetramers with 0- and 2-bp spacers have different quaternary structure. When superimposing the 0 and 2 bp tetramer from crystal 1, monomer B superimposes with monomer J, but the other three monomers are shifted.

Table S1. Data collection and refinement statistics

	Crystal 1	Crystal 2	Crystal 3
	12 bp (PDB: 3VD0) 5′-CAGGCATGCCTG-3′	12 bp (PDB: 3VD1) 5′-CGGGCATGCCCG-3′	14 bp (PDB: 3VD2) 5′-ATGGACATGTCCAT-3′
Data collection			
Space group	$P2_1$	$P2_1$	$C2$
Cell dimensions			
a, *b*, *c*, Å	82.09, 104.52, 122.99	82.54, 104.20, 123.22	158.40, 91.12, 137.47
β, °	96.18	96.50	90.20
Resolution, Å	100–2.95 (3.0–2.95)	100–2.95 (3.06–2.95)	100–4.00 (4.14–4.00)
R_{sym} or R_{merge}	7 (37)	6 (40)	12.5 (40.2)
$I/\sigma I$	16.5 (4.54)	20.1 (3.2)	10.6 (3.8)
Completeness, %	99.9 (99.6)	96.1 (96.5)	99.6 (99.2)
Redundancy	5.4 (5.5)	6.2 (5.7)	5.9 (5.6)
Refinement			
Resolution, Å	20.0–2.95	20.0–2.95	45.5–4.0
No. reflections	43,405	41,779	16,649
R_{work}/R_{free}	23.5/25.4	23.9/28.5	24.8/28.4
No. of molecules in asym. unit			
Protein/dsDNA	8/4	8/4	6/3
No. atoms	15,005	15,149	11,435
Protein	12,691	12,584	9,483
DNA/Zn^{2+} ion	1,871/8	1,944/8	1,675/6
Water	233	326	-
B factors	75.0	72.7	86.6
Protein	74.6	71.6	83.4
Ligand/ion	88.3/61.1	84.8/57.9	104.5/76.3
Water	43.2	42.9	—
Rms deviations			
Bond lengths, Å	0.008	0.009	0.01
Bond angles, °	1.6	1.7	1.9
Ramachandran Plot, %			
Res. in most favored reg.	82.3	78.6	73.8
Res. in additional allowed reg.	17.0	20.8	25.0
Res. in generously allowed reg.	0.7	0.6	1.2
Res. in disallowed reg.	0.0	0.0	0.0

Values in parentheses are for highest-resolution shell. PDB, Protein Data Bank; Res., residues; reg., region.